 https://doi.org/10.3011/ESARDA.IJNSNP.2017.14

Outcomes of the JNT 1955 Phase I Viability Study of Gamma Emission Tomography for Spent Fuel Verification

S. Jacobsson Svärd[1], L.E. Smith[2], T.A. White[2,7], V. Mozin[3], P. Jansson[1], P. Andersson[1], A. Davour[1], S. Grape[1], H. Trellue[4], N. Deshmukh[2], E.A. Miller[2], R. S. Wittman[2], T. Honkamaa[5], S. Vaccaro[6], J. Ely[7]

1 Uppsala University, Uppsala, Sweden
2 Pacific Northwest National Laboratory, Richland, WA, USA
3 Lawrence Livermore National Laboratory, Livermore, CA, USA
4 Los Alamos National Laboratory, Los Alamos, NM, USA
5 STUK – Radiation and Nuclear Safety Authority, Helsinki, Finland
6 European Commission, Directorate General Energy, Directorate Euratom Safeguards, Luxembourg
7 International Atomic Energy Agency, Vienna, Austria

Abstract:

The potential for gamma emission tomography (GET) to detect partial defects within a spent nuclear fuel assembly has been assessed within the IAEA Support Program project JNT 1955, phase I, which was completed and reported to the IAEA in October 2016. Two safeguards verification objectives were identified in the project; (1) independent determination of the number of active pins that are present in a measured assembly, in the absence of a priori *information about the assembly; and (2) quantitative assessment of pin-by-pin properties, for example the activity of key isotopes or pin attributes such as cooling time and relative burnup, under the assumption that basic fuel parameters (e.g., assembly type and nominal fuel composition) are known. The efficacy of GET to meet these two verification objectives was evaluated across a range of fuel types, burnups and cooling times, while targeting a total interrogation time of less than 60 minutes.*

The evaluations were founded on a modelling and analysis framework applied to existing and emerging GET instrument designs. Monte Carlo models of different fuel types were used to produce simulated tomographer responses to large populations of "virtual" fuel assemblies. The simulated instrument response data were then processed using a variety of tomographic-reconstruction and image-processing methods, and scoring metrics were defined and used to evaluate the performance of the methods.

This paper describes the analysis framework and metrics used to predict tomographer performance. It also presents the design of a "universal" GET (UGET) instrument intended to support the full range of verification scenarios envisioned by the IAEA. Finally, it gives examples of the expected partial-defect detection capabilities for some fuels and diversion scenarios, and it provides a comparison of predicted performance for the notional UGET design and an optimized variant of an existing IAEA instrument.

Keywords: Spent nuclear fuel assemblies; Partial defect verification; Gamma-ray emission tomography

1. Introduction

The accurate verification of declarations about the fissile content of spent fuel is central to the International Atomic Energy Agency's (IAEA) safeguards of facilities handling and storing irradiated fuel. IAEA safeguards approaches for used fuels that are being transferred to difficult-to-access storage and that have a design allowing disassembly call for verification using a partial-defect or best-available method [1]. At present, IAEA's authorized instruments for attended partial-defect detection have limitations in terms of independence, defect sensitivity, and implementation flexibility. Furthermore, there is no authorized instrument for unattended partial-defect detection in spent fuel. Accordingly, the IAEA has expressed a need for "more sensitive and less intrusive alternatives to existing NDA instruments" for partial-defect detection [2].

Passive gamma-ray emission tomography (GET) is attractive for addressing partial-defect detection because it has the potential to non-destructively image the spatial distribution of the active fuel material in the assembly structure, and extract numerical data on individual fuel pins, without the need for any operator-declared information or disassembly of the fuel. Advantage is taken of the high level of radioactivity in used nuclear fuel in a two-step procedure:

(i) The gamma radiation field around a fuel assembly, at a selected axial level, is collected using one or several gamma-ray detector elements in a large number of positions relative to the fuel, and;

(ii) The internal source distribution in the fuel is reconstructed based on the recorded data, using tomographic algorithms.

In both steps, one may identify a multitude of alternative approaches, e.g. in terms of choice of detector set-ups and measurement schemes (step i) and choice of data analysis and reconstruction algorithms (step ii). In addition, for the case when the assay result is an image, there is a variety of image-analysis methods that may be applied to draw conclusions on the individual fuel pin level.

As described in this paper, reconstructed images and pin-wise data may be used directly to draw conclusions on possible pin diversion. Measured gamma-ray source

 Jacobsson Svärd, S., Smith, L.E., White, T.A., Mozin, V., Jansson, P., Andersson, P., Davour, A., Grape, S., Trellue, H., Deshmukh, N., Miller, E.A., Wittman, R.S., Honkamaa, T., Vaccaro, S., & Ely, J. (2017). Outcomes of the JNT 1955 Phase I Viability Study of Gamma Emission Tomography for Spent Fuel Verification. *ESARDA Bulletin - The International Journal of Nuclear Safeguards and Non-proliferation*, 55, 10-28. https://doi.org/10.3011/ ESARDA.IJNSNP.2017.14

concentrations can also be strongly correlated to fuel parameters such as burnup (BU) and cooling time (CT), thereby achieving more specificity than other partial-defect detection methods. Further, tomographic assessment at multiple axial locations along the assembly length enables axially resolved pin-level assay (as opposed to volume-integrating assay). Finally, GET is viable in both wet and dry measurement environments, and in either unattended or attended modes, thus offering operational flexibility.

The IAEA attention to the GET technique began in the 1980's, leading to the development and testing of small-scale systems in multiple field campaigns on BWR and PWR fuel items [3]. Building on those efforts, the JNT A 1510 project began in 2003 and was completed in late 2015. Under JNT 1510, a full-scale, transportable tomography system based on IAEA's user requirements for underwater application was designed, fabricated, and field-tested [4]. This system is referred to as PGET (Passive Gamma Emission Tomography) and is used in attended mode.

In parallel to the IAEA-led efforts, a Swedish project for validating core simulators for pin-power distributions led to the construction of a heavy (30-metric tons) tomographic device, which was used for measurements on short-cooled (2-4 weeks) BWR fuel assemblies [5], [6]. As a consequence, the project also covered studies of the safeguards aspects of this technique [7]. During recent years, international nuclear research institutes have also gained interest in the application of tomographic techniques on complete fuel assemblies [8], [9]. Leveraging from the relatively large pool of knowledge and expertise that is now available on GET, the JNT 1955 Phase I project was launched by the IAEA in 2013 and was reported on in 2016 [10]. This paper accounts for its main outcomes.

2. Scope of the JNT 1955 Phase I project

The JNT 1955 Phase I project was carried out in 2013-2016 by the IAEA Member States Support Programs of the United States, Sweden, Finland and European Union, under the leadership of the IAEA. It was intended to complement previous IAEA projects on the GET technique, e.g. by considering unattended GET and an extended range of fuels and implementation scenarios.

Verification Objective	Description	Assumptions
1	Independent determination of the number of active pins that are present in a measured fuel assembly.	No a priori information about the assembly is available.
2	Quantitative assessment of pin-by-pin properties, for example the activity of key isotopes or pin attributes such as cooling time (CT) and relative burnup (BU).	Basic fuel parameters (e.g., assembly type, geometry and nominal fuel composition) are known.

Table 1: Verification Objectives covered in the JNT 1955 Phase I project.

At the project start-up, two Verification Objectives were identified, as defined in Table 1, where only Objective 1 may be considered addressed by the already existing PGET device. With these Verification Objectives in mind, efforts were made within the following areas:

- **GET performance analysis framework:** A modelling and analysis framework was developed for partial-defect detection capability evaluation, including a procedure for simulating tomographic data for selected experimental setups, fuel types, diversion and implementation scenarios;
- **GET instrument design:** The design of a "universal" GET instrument (UGETv1) was developed, intended to support the full range of verification scenarios envisioned by the IAEA;
- **Reconstruction and analysis methods:** A set of tomographic reconstruction and analysis methods were identified, described and demonstrated;
- **Proposed metrics for GET partial-defect sensitivity:** Metrics for quantifying the partial-defect detection capability of alternative GET approaches on selected diversion cases were suggested;
- **Quantitative performance predictions:** Quantitative performance predictions were made for the PGET and UGETv1 instrument designs, for a set of different fuel types, fuel parameters and diversion scenarios;
- **Inspection procedures:** An envisioned inspection procedure was presented.

Due to the extent of the work, each area is only covered superficially in the coming sections of this paper, while details may be found in [10].

3. GET performance analysis framework

One important outcome of the JNT 1955 project is the creation of a modelling and analysis framework for the evaluation of GET partial-defect-detection performance, which can be applied to various GET instrument designs, fuel assembly types and parameters, diversion scenarios and analysis methods. A flowchart describing this framework is illustrated in Figure 1. It provides end-to-end capability to assess tomographer performance for nuclear fuel assay, and could be considered a new, standing capability for the international safeguards community.

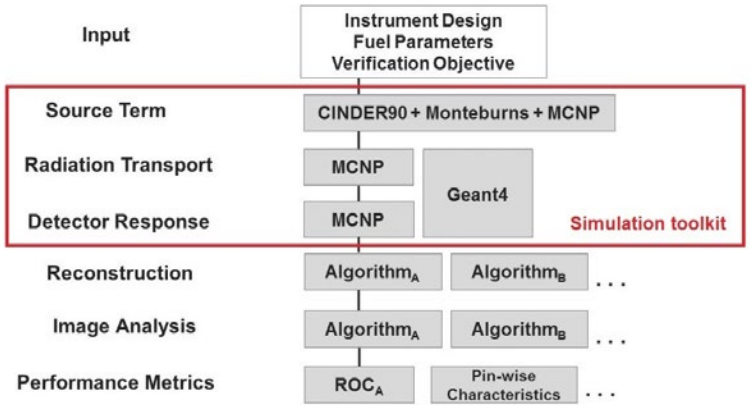

Figure 1: Flowchart describing the modelling and analysis framework developed for GET performance evaluation.

The inputs are the specifics of the fuel to be analyzed, the instrument design, including data-collection schemes such as the set of angular and lateral detector element positions used, and the conditions under which the analyses are made (e.g. the level of access to a priori information), which governs the tomographic reconstruction and analysis methods that are applicable. (Verification Objectives 1 and 2 presented in Table 1 are examples of such conditions.) The framework allows for the deployment of various reconstruction and analysis methods as well as various metrics of performance.

The heart of the framework is the simulation toolkit, marked in red in Figure 1. Here, a brief overview of the simulation procedure is presented, and the reader is referred to ref. [10] for more details;

1. First, pin-by-pin gamma-ray source terms for each fuel type and fuel parameter set under study are calculated using a combination of codes and methods, as described in refs. [11] and [12].
2. Second, the Monte Carlo N-Particle (MCNP) transport code [13] is used for transport of emitted gamma quanta from the fuel to the surface of the detector elements, taking into account the specifics of the fuel geometry studied (including possible pin diversions) and the device design. To allow for acceptable computation times for the low-efficiency transport geometries of this study, semi-deterministic transport is deployed; using MCNP's next-event estimator method, the probability of the gamma-ray contributing to a point at the front face of the detector is calculated analytically at each interaction or source point. Consequently, variations in response to gamma quanta hitting different parts of the detector surface are neglected, which is justified by the fact that the front surface of all detectors in this study was much larger than the exposed area, as defined by the collimator slit opening. These calculations are done pin-by-pin and energy-by-energy to get single-pin flux data for the complete set of detector element positions, which can be added together to form complete assembly data. In this summation, pin-wise weights are applied according to the source terms calculated in the first step. (In this way, the results from the time-consuming transport calculation can be re-used when changing pin-wise fuel parameters.) In this work, alternative simulations using the Geant4 code [14] have also been performed to benchmark the MCNP simulations, as described in section 7.2.
3. Third, separate Monte Carlo calculations of the detector response are performed, taking into account the complete gamma-ray flux into the detector elements, at all energies, while also considering detector specifics (e.g. energy resolution). Consequently, performance of different detector types in the same setup can be assessed using the same data from the first two steps.

This three-step simulation procedure allows for the creation of tomographic data for large virtual assembly populations, in terms of; (i) varying pin-by-pin BU, and; (ii) varying sets and levels of statistical noise. The former variation responds to the fact that authentic fuel assemblies have a pin-by-pin variation in BU. (In BWR fuels in particular, there may be relatively large variations in pin-wise BU due to spatial variations in void and thus in thermal neutron flux, which is met to some extent by introducing variations in initial enrichment. According to BWR operators, the maximum variation in pin-wise BU may be as large as ±20% under normal operation [15], [16].) The latter variation allows e.g. measurement time to be accounted for. Altogether, analyses of large assembly populations, with these variations included, enable the deployment of statistical performance metrics, as discussed in section 6.

4. GET instrument design

The data used for emission tomography consists of a set of gamma-ray intensities that should be recorded in well-defined angular and lateral positions with respect to the object. For the reconstructions to be efficient, a small region of the object should contribute to the recorded intensity in each position, as defined by the angle under which the radiation travels and the lateral distance of the region from the centre of rotation. In this application, heavy

collimators are used, which shield the detector elements while allowing radiation to enter through well-defined slit openings, thus allowing for the required spatial selection capability. The collimator-detector setup may be arranged in a rotate-only geometry or in a rotate-translate mechanical arrangement. The achievable spatial resolution will be governed by the system's spatial response, which is defined primarily by the slit openings, in combination with the lateral distance between each data point. (In a rotate-only geometry, the lateral distance is defined by the collimator pitch, while in a rotate-translate geometry, it is defined by the translation step used).

In the instrument design, the choice of detector as well as collimator material and dimensions depend on a number of factors such as;

– Fuel properties, e.g. BU, CT and size: Highly radioactive fuel (short CT, high BU, large mass) generally requires better shielded detector elements to avoid high levels of background radiation. Here, one may foresee a background of gamma quanta from other axial levels of the assembly than the one measured if shielding is inadequate, and gamma quanta entering the detector elements after being scattered in surrounding materials may also pose a problem;
– Requirements on isotopic selectivity: Detector elements with high energy resolution and spectroscopic data collection may be required to select specific gamma peaks, in particular for Verification Objective 2. Also, high full-energy peak efficiency will enable more efficient subtraction of background from scattered gamma rays, and thus enhanced data quality;
– Spatial resolution requirements: Longer and/or narrower collimator slits enable higher spatial resolution. (As pointed out above, spatial resolution is also governed by the measurement scheme used, in particular the lateral distance between data points.);
– Count-rate management: The collimator slit dimensions should preferably be large enough to allow for high counting rates in order to reduce measurement time, while staying within acceptable limits for the selected detector type in terms of count-rate saturation;
– Time requirements: Assay time can be shortened by using many, tightly-packed, detector elements as well as using detectors with high-count-rate capability.

Altogether, there is a strong inter-dependence between these design factors. As an example, detector elements offering high full-energy peak efficiency are generally relatively large, implying that a relatively small number of detectors will fit into the device, thus leading to longer assay times. Accordingly, instrument design will include a trade-off between e.g. time and precision.

The device design performed in this work was developed to meet both Verification Objectives 1 and 2, resulting in the notional Universal GET design (UGETv1). Thorough presentations of the UGETv1 design and the considerations made can be found in refs. [10] and [17], and only the outcome of the design work is presented here. The design was informed by two previous underwater designs, PGET [4], which was constructed in the JNT 1510 project to deliver on Verification Objective 1 for relatively long-cooled fuel, and PLUTO [6], which was constructed in Sweden to deliver pin-wise power in short-cooled fuel, a task similar to Verification Objective 2. The PGET and UGETv1 designs are illustrated in Figure 2, and their respective properties are listed in Table 2.

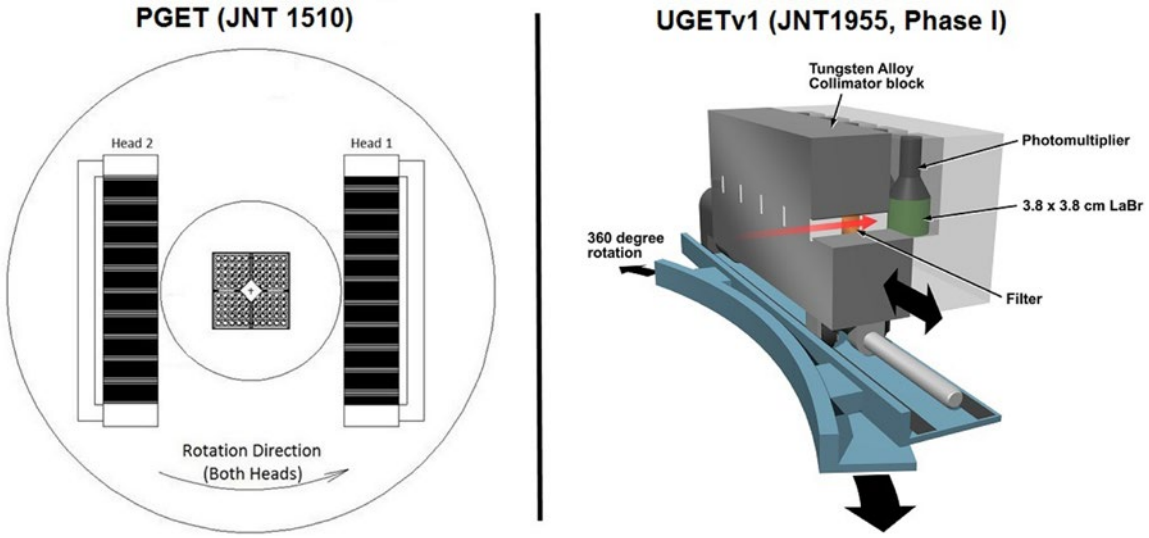

Figure 2: The two device designs analysed in section 7. **Left:** The existing PGET device, which was constructed in the JNT1510 project. It is based on two large arrays of small CdTe detectors, operated in threshold mode, in a rotate-only geometry. **Right:** A single detector head of the notional UGETv1 design, developed in this work. The full instrument would include four heads, each housing 8 relatively large $LaBr_3$ detectors operated in spectroscopic mode, in a translate-rotate geometry. The devices are not to scale.

Design parameter	PGET*	UGETv1
Maximum object diameter	30 cm	37.5 cm
Number of detector heads	2	4
Number of detectors per head	104	8
Detector type	CdTe	$LaBr_3$§
Detector dimensions	Cuboid: 10×5×2 mm^3	Cylindrical: 38x38 mm
Spectroscopic analysis	Broad Region-Of-Interest (ROI)	Peak analysis
Collimator slit length	100 mm	200 mm
Collimator slit width	1.5 mm	1.5 mm
Collimator slit height	Tapered 70→10 mm	10 mm
Detector (and slit) pitch	4 mm	46 mm
Number of lateral steps per angular projection for 2 mm sampling	- (rotation only)	23

* PGET parameters reflect design under JNT 1510. During 2016, PGET was refurbished, changing the design slightly.

§ LaBr3 scintillators are generally doped with small portions of Cerium to activate photoemission.

Table 2: Parameters of the existing JNT1510 PGET and the notional JNT1955 Phase I UGETv1 device designs.

As described in section 7, performance evaluations have been carried out for the PGET and UGETv1 designs. In short, the main differences between these designs and assumed modes of operation are; (i) the existing PGET device operates relatively small CdTe detectors in threshold mode with limited full-energy detection efficiency at high energies, while the notional UGETv1 design is intended to host larger $LaBr_3$ scintillator detectors, for which the evaluations assume spectroscopic full-energy gamma-ray peak analysis, and; (ii) PGET uses relatively light collimation, while additional shielding is included in UGETv1 to manage count rates for more short-cooled fuels (CT down to 1 year). As a result of these design selections, PGET allows for tightly-stacked detector arrays that offer rapid data collection in a rotate-only geometry, while the fewer number of $LaBr_3$ detectors in UGETv1, which offer more isotopic-specific data by means of size and mode of operation, require both rotation and translation of the detector arrays to record complete intensity projections, leading to longer assay times.

5. Reconstruction and analysis methods

Once the tomographic data have been recorded, tomographic reconstruction algorithms are applied to calculate the internal source distribution. There are a variety of algorithms available for emission tomography, which over the years have been developed and applied mainly for medical applications. However, a nuclear fuel assembly, with its highly inhomogeneous mix of strongly gamma-ray attenuating materials (such as uranium dioxide) and less attenuating materials (such as water or air), is a challenging object for tomographic measurement and reconstruction. If not taken into account in the reconstructions, gamma-ray attenuation will strongly influence the resulting representation of the source distribution. In this work, options from the two main classes of tomographic reconstruction algorithms; analytic and algebraic [18], have been explored for use on nuclear fuel assemblies. Analytic methods, such as filtered back-projection (FBP), typically use the Fourier transform, while the algebraic methods express the reconstruction in terms of an equation system, allowing for detailed modelling of e.g. attenuation when defining the equation system's weight matrix (the system matrix). The quantitative capabilities of some analysis methods when applied on emission data from nuclear fuel assemblies are presented in ref. [19].

The data used for tomographic reconstruction may constitute either of peak-specific data, giving information on the contents of the isotope emitting that particular peak, or of data that comprise a mix of information from several peaks and various levels of scattered gamma rays, depending on the instrumentation and the settings used for the data acquisition. In the end, the reconstructions will create information of the source distribution, but the specificity of this information will depend on the quality of the input data. In this section, the principles used for the tomographic reconstructions are described, while examples of output from devices with different hardware and settings are presented in section 7.

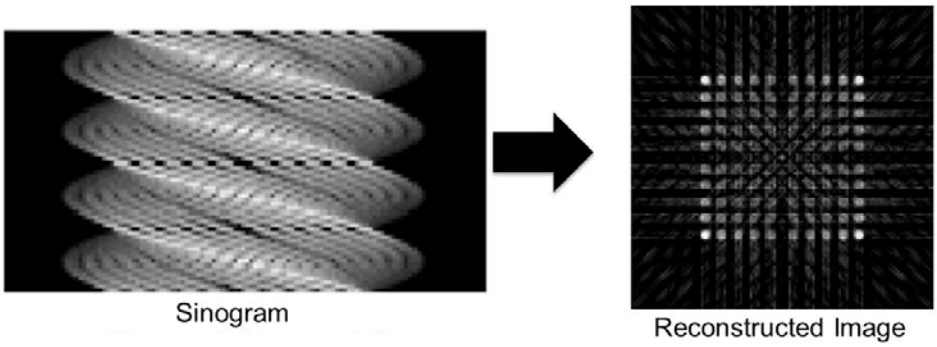

Figure 3: Tomographic data may be presented as a sinogram, with intensities as a function of lateral detector element position (horizontal axis) and angular position (vertical axis). Image reconstruction methods transform sinogram data into images of gamma-ray emission intensity, which are further analysed to deduce pin-wise data. (Example data obtained by simulating the detection of gamma rays in a 400-700 keV interval, being dominated by ^{137}Cs, modelling BWR fuel in the JNT1510 PGET instrument design.)

5.1 Image reconstruction and image analysis for Verification Objective 1

For Verification Objective 1, the number of fuel pins present should be determined without assuming any *a priori* information on the fuel. The route taken in this case is to reconstruct an image of the axial cross section of fuel, based on the collected sinogram of a fuel assembly (i.e. the collected intensities in a set of angular and lateral detector element positions relative to the fuel), see Figure 3. This image is then further analysed to deduce pin-wise data and allow for counting of the fuel pins.

Most image reconstructions in this work have been done using a standard FBP algorithm [18]. One may note that this type of algorithm does not include any attenuation corrections, and implicitly assumes an ideal spatial response function (i.e. the intensity in the detector is assumed to emanate from an infinitesimally thin line through the object). As an alternative, some reconstructions have also been performed using an algebraic method, modelling the spatial response of the collimator-detector system and assuming homogeneous attenuation in the image area when defining the system matrix [19]. With this method, a more realistic physics representation is achieved using no prior fuel information, thus fulfilling the assumptions for Objective 1. The spatial response function of the UGETv1 design used for 1274 keV gamma rays is presented in Figure 4.

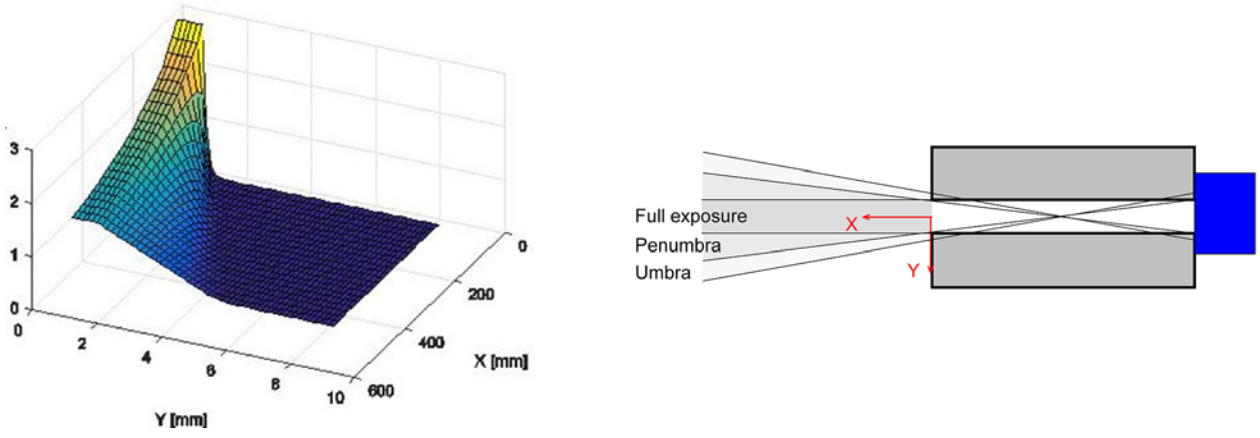

Figure 4: An example spatial response function for 1.274 MeV gamma rays (a.u. on the z axis) of the UGETv1 device design, used in algebraic reconstructions (left figure). The origin (X,Y=0) of the response function is centred at the front of the slit opening, and only positive Ys are presented. The function takes into account the physical properties of the measurement system (e.g., in terms of finite collimator slit width and gamma-ray transmission through the collimator material), which give rise to significant contributions from penumbra and umbra regions, illustrated schematically in the right figure. (For actual slit dimensions, see Table 2.)

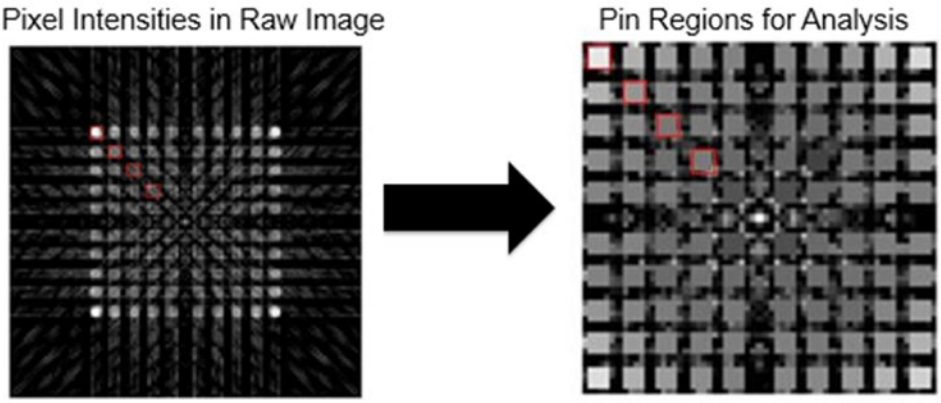

Figure 5: Example reconstructed image of simulated data for a VVER-440 assembly (left). The most fundamental image analysis is the aggregation of pixel intensity values in beforehand-defined pin-centred quadratic regions (right). A toolkit of more advanced image-analysis methods have also been developed to search the image for pins, being capable of adapting to possible irregularities in the geometry, as presented in ref. [20]. (Example images, obtained in reconstruction of simulated data from BWR fuel in the JNT1510 PGET instrument design. Here, the detection of gamma rays in a 400-700 keV ROI was modelled, being dominated by ^{137}Cs.)

Once the image is obtained, image analysis methods are required to extract pin-by-pin data, here called "pin scores". The most fundamental image analysis is to aggregate the reconstructed activities of multiple pixels in a "neighbourhood" centred on each pin location, as illustrated in Figure 5. However, irregularities that may arise from e.g. assembly torsion and pin dislocations may call for more advanced methods. A toolkit of such methods has been developed for analysis of fuel assembly images [20]. As part of the JNT1955 Phase I project, these methods were demonstrated on experimental tomographic images, proving functional on disturbed geometries [10].

Examples of analysis results for PGET and UGETv1 are given in section 7 for two combinations of methods; (i) FBP reconstruction and fundamental image analysis; and (ii) algebraic reconstruction and advanced image analysis. All analysis codes used can be made available to the IAEA.

5.2 Pin-activity reconstruction for Verification Objective 2

For Verification Objective 2, pin-wise fuel properties should be determined under the assumption that information on the fuel and its geometry is available. This opens a possibility to apply detailed modelling of the fuel configuration using algebraic methods, enabling a level of detail not accessible using analytic methods. In the work on Objective 2, three different alternatives have been used for defining a detailed system matrix in algebraic reconstructions, for which software can be made available to the IAEA; (Results obtained using t Wayfinding he two latter methods are presented in section 7.4.)

– **MCNP-generated matrix:** For simulation data obtained using MCNP (see section 3), the same transfer function as was used to create the data may be used to reconstruct the modelled source distribution. While being "unrealistically perfect" for the simulated data set, this approach enables analyses of the sensitivity to stochastic noise, added to the simulated data. For experimental data, one may also envisage the use of MCNP or similar Monte Carlo codes to model the system matrix, however, such a procedure would be excessively slow for "new" measured cases.
– **Ray-tracing:** The reconstruction toolkit TOMOPACK, with established use for reconstructions of tomographic data from the PLUTO [5] and Halden [9] devices, where %-level precision of pin-wise data has been demonstrated, is essentially based on ray-tracing and is thus suitable for analysis of spectroscopically-analysed full-energy-peak data. This modelling comprises the following features; (i) modelling of the instrument's spatial response function, see Figure 4; (ii) modelling the full-energy gamma-ray transport through the detailed 3D configuration of fuel pins, taking the axial symmetry into account, and; (iii) adaption of the pixel pattern to fit the object.
– **RADSAT-based matrix:** The Radiation Detection Scenario Analysis Toolbox (RADSAT) [21] combines 3-D deterministic transport through the measurement geometry with a stochastic model for detector response. Its use for tomography is somewhat exploratory, but it offers the capability to generate object-scatter contributions in the system matrix coefficients, for each pin, which may be essential for the analysis of data with low full-energy peak specificity, such as that of PGET.

6. Proposed metrics for GET partial-defect detection capability

For Verification Objective 1, so-called receiver operator characteristic (ROC) curves are suggested to provide metrics of the partial-defect detection capability, since they can be used to understand the trade-off between probability of detection (PD) and probability of false alarm (PFA). ROC analysis is used in many fields; a standard reference from

imaging sciences relevant to this work can be found in [22]. In the present case, the pin scores obtained from a measurement (calculated as described in Section 5.1) can be plotted as histograms, one histogram for the pins present and another for pins missing (or replaced). In the ROC analysis, a threshold value is selected, so that pin scores above the threshold are defined as pins present, while scores below the threshold are defined as non-fuel objects. If the two histograms do not overlap, perfect detection of missing pins without any false alarms can be realised. If the histograms overlap, then false alarms and/or non-detected missing pins will occur, depending on the threshold. By varying the threshold, the tradeoff between detection and false alarm can be quantified. An example of how the pin-score distributions for pins missing and pins present can be used to generate a ROC curve is given in Figure 6. When selecting an acceptable false alarm rate (setting the threshold), the ROC curve will give the corresponding probability of detection.

For Verification Objective 2, the metric used in this work (see e.g. section 7.4) is simply the agreement of reconstructed pin-wise isotopic activities with the simulated source distribution, expressed as a relative difference, or "fractional error". At the event of inspection, pin-wise data measured using a benchmarked methodology may be used to verify operator-declared data (in case such are available on the individual pin level) or to evaluate consistency among the population of pins in an assembly at a level within the demonstrated precision.

7. Quantitative performance predictions of PGET and UGETv1 device designs

Using the modelling and simulation framework described in section 3, the expected performance of two device designs has been analysed; the existing PGET device and the notional UGETv1 device (see section 4). The reconstruction tools described in section 5 have been deployed, as well as the performance metrics described in section 6.

7.1 Analysed cases

Since the number of imaginable GET implementation alternatives and diversion scenarios are exceedingly large, and a vast amount of time is required for simulating each foreseeable case, a comprehensive study of all possibilities would not be manageable. Consequently, this study was limited to a relatively small set of implementation and pin-diversion scenarios, fuel types and parameters, and gamma-ray energies used for assay, according to the following;

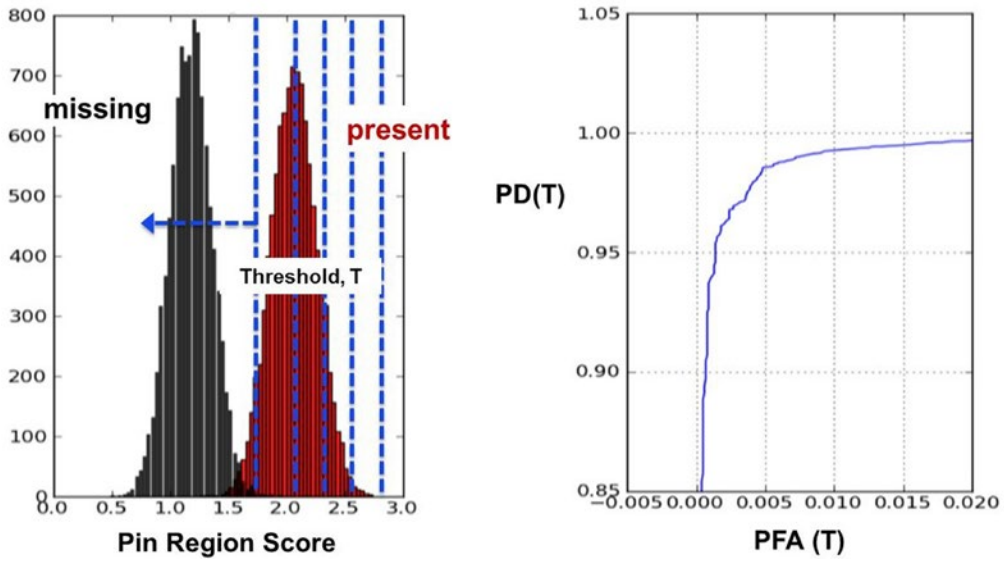

Figure 6: Pin-score distributions for pins missing and pins present (left) can be used to calculate the probably of detection (PD) and probability of false alarm (PFA) as a function of threshold, T, in terms of a ROC curve (right).

Implementation scenarios: The matrix of implementation scenarios (including fuel CTs), deployment constraints and target measurement times considered in this work is presented in Table 3. The notional UGETv1 device covers a CT range from 1 to 40 years, while PGET is not applicable for CTs as short as 1 year. Measurement times up to approximately 60 minutes were assumed acceptable. Only underwater assay was studied.

Pin-diversion scenarios: Three partial defect scenarios were considered; (i) Pin removal without any substituting materials, i.e. with water replacing the pins; (ii) Pin replacement with depleted-uranium pins (replicates low- or no-activity containing high-density substitute), and; (iii) Pin replacement with fuel pins of the same construction but lower BU (replicates material diversion between reactor cycles). However, as described in [10], scenario (ii) poses the least tomographically challenging case. Focusing on the

more challenging cases, only results from scenarios (i) and (iii) are presented here.

Fuel types, parameters and pin configurations: Three fuel types were studied, for which the simulated fuel pin configurations are illustrated in Figure 7; (i) SVEA-96S BWR fuel with 96 fuel pins, of which 5 were diverted; (ii) VVER-440 fuel with 1 water channel and 126 fuel pins, of which 6 were diverted, and; (iii) PWR 17x17 fuel with 25 water channels and 264 fuel pins, of which 11 were diverted. Due to gamma-ray attenuation, it is more challenging to tomographically measure fuel types with large and dense pin configurations, where information obtained from central fuel pins is scarce. Accordingly, BWR fuel poses the least challenging configuration and PWR poses the most challenging. Fuel BUs from 10 to 40 GWd/MTU were analysed in order to span typical values encountered in commercial power industry.

Gamma-ray energies: The gamma-ray source terms will depend on the fuel parameters; short-cooled assemblies will contain short-lived as well as long-lived fission products and higher total activity, while the gamma-ray spectrum emitted from long-cooled assemblies (CT>30 years) will be dominated by ^{137}Cs. All simulations covered a large number of gamma emitters and energies, but in the tomographic analyses only a few energy regions were selected (taking detector characteristics into consideration), corresponding to specific gamma-emitting fission products. The gamma-ray energies under study in this work are presented in Table 4. For each gamma-ray energy, relevant stochastic noise levels corresponding to assay time, BU and CT, were included in the statistical analyses of each simulated fuel type. The noise levels were given by Poisson statistics, based on simulated absolute intensities.

Implementation Scenario	Cooling time (years)	Deployment constraints
Routine verification of old fuel being transferred to a geologic repository	40	Attended or unattended
Routine verification of fuel being transferred to dry storage	5	Attended or unattended
Random verification of in-pool inventory	1	Attended

Table 3: Description of GET implementation scenarios considered in this work. The hardware configurations studied were the existing PGET device and the notional UGETv1 design (see section 4), for both Verification Objective 1 and Objective 2.

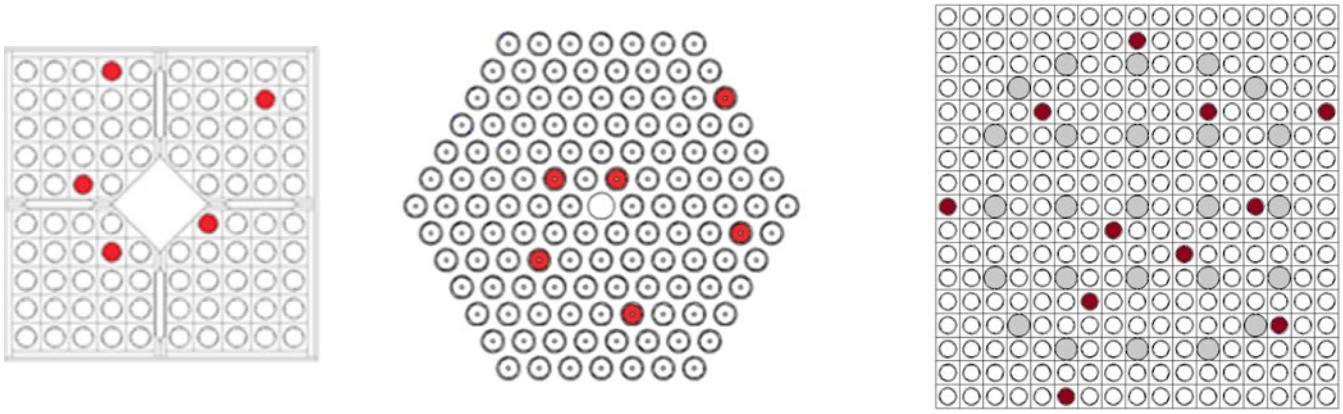

Figure 7: Map of the simulated diverted pin locations (in red) in the three assembly types under study: five for BWR (left), six for VVER-440 (middle) and 11 for PWR (right). In addition, VVER fuel by design includes one central water channel and PWR fuel includes 25 water channels (marked in grey). The fuel geometries are presented approximately, but not exactly, to scale.

Isotope	Energy [MeV]	Branching ratio [%]	Half-life	Relevant CT range
^{137}Cs	0.662	85.1	30.1 y	up to 100-150 y
^{134}Cs	0.605	97.6	2.1 y	up to 10 y
	0.796	85.5		
^{154}Eu	0.723	20.1	8.6 y	up to 25–30 y
	0.873	12.1		
	0.996	10.5		
	1.005	18.0		
	1.274	34.8		
^{144}Pr (^{144}Ce)	2.186	0.7	285 d	up to 5 y

Table 4: Characteristic fission products and associated gamma-ray emissions from spent fuel in the 0.4-2.5 MeV energy region. (Data from [23])

In general, the higher gamma-ray energies in Table 4 facilitate tomographic assay, since their higher penetrability enables more information to be obtained from the assemblies' innermost sections. However, also the emission intensity is important. For ^{154}Eu, the highest energy (1.274 MeV) is also the most intense and thus the most useful. One should note that for relatively long-cooled fuel (CT between 30 and about 100 years), only the long-lived, lower-energy gamma emitter ^{137}Cs is abundant enough to be measured.

7.2 Simulation and benchmarking

The simulation toolkit described in section 3 was used to create tomographic data for sets of virtual fuel assemblies for the cases accounted for above. For all simulations, all gamma quanta interacting in the detector elements were analysed with respect to their energy deposition, and the number of events in selected energy ROIs were analysed. The settings used for simulating the PGET device are presented in Table 5. For the notional UGETv1 device, spectroscopic full-energy peak analysis including subtraction of background under the peaks was assumed, and the detection of a set of individual emission lines in a small energy interval (few keV) about each peak was simulated.

ROI [keV]	Comment
400-700	Used for analysis of 662 keV gamma from ^{137}Cs
700-1100	Used for analysis of ^{154}Eu (primarily lines at 723, 873, 996, and 1005 keV)
1100+	Used for analysis of 1274 keV gamma from ^{154}Eu

Table 5: The Regions-Of-Interest (ROI) used when simulating PGET data. In the simulations, the energy deposition in the detector elements were analysed, while counting the number of events falling within the ROIs.

Following the procedure described in section 3, "single-pin base sinograms" were weighted and added together to comply with isotopic contents due to selected pin-wise BU and CT. Accordingly, high statistical quality of these "base data" was critically important for reducing systematic effects in the large sets of derived virtual assemblies that were used to assess performance evaluation. A particular concern was the sampling of pin contributions from the inner regions of the assembly, where gamma-ray self-shielding and line-of-sight obstructions are severe, leading to few sinogram counts. However, the calculation scheme did not allow for statistical analyses of individual single-pin sinograms. Instead, an estimate of precision emanating from the "base data" was achieved using two separate, independent simulations, according to a procedure described in [10]; In short, a "difficult case" (low gamma-ray energy from ^{137}Cs in a large PWR fuel configuration) was selected, for which tomographic data was obtained by aggregating "base data" respectively by performing an independent, high-level-statistics simulation of a complete fuel assembly with corresponding pin-wise ^{137}Cs contents. The two sets of data were used in identical reconstructions, and the differences in reconstructed pin-wise data were interpreted as imprecision emanating from the "base data". It was found that fuel pins near the assembly periphery were reconstructed at almost identical values for the two data sets, whereas differences increased towards the assembly centre, as expected. For all fuel pins the differences were within maximum ±3%, giving an indication of the precision of the base data and thus defining a limit of the achievable agreement of reconstructed pin-wise data to simulated source contents for this "difficult case". One may note that implications of counting statistics, due to e.g. variations in detector count rate or measurement time, may be evaluated at a higher level of precision by investigating the statistical spread obtained when adding such variations to the base data.

In order to ensure that the simulation-based conclusions drawn on PGET and UGETv1 performance for various fuel parameters and measurement times are correct, the Monte Carlo simulations were verified and validated in multiple ways;

- Gamma-ray source terms and detector response calculations (simulation steps 1 and 3 of Section 3) were evaluated using experimental data from measurements performed at the Clab interim storage facility for spent fuel in Sweden. This benchmark included relative peak intensities for a large number of gamma peaks as well as peak shape and level of Compton-scattered background;
- The Monte Carlo-based gamma-ray transport (simulation step 2 of Section 3) was evaluated using experimental tomographic data from the PLUTO device [5]. Both simulated gamma-ray projections as well as properties of reconstructed images were evaluated;
- The MCNP model of the PGET device was evaluated using experimental PGET data;
- A model of the PGET device was also developed in the alternative Monte Carlo simulation tool Geant4, and the Geant4 simulations were evaluated using experimental PGET data, and;
- The MCNP model of the notional UGETv1 device was evaluated in inter-code simulation comparisons to an independent Geant4 model.

All evaluations were considered satisfactory, thus providing confidence in the comparisons made between expected instrument performance for the existing PGET and the notional UGETv1 devices. Details on the evaluations can be found in ref. [10].

7.3 Results for Verification Objective 1: Independent pin counting

As accounted for in section 5.1, the approach for Verification Objective 1 was to use tomographic data in different types of image reconstructions, and perform image

analysis on the reconstructed images to independently count the number of fuel pins. Two alternative analysis routes were taken:

– **Analysis Route 1:** Basic analytic FBP image reconstruction, followed by basic image analysis (summing sets of pixel values said beforehand to represent each fuel pin). While not allowing for inclusion of spatial response or gamma-ray attenuation in the reconstruction, nor adaption to possible dislocation or torsion of the fuel in the image analysis, this route enabled automated analysis of large populations (up to 1,000) of simulated assemblies with varying BU distributions and stochastic noise. Consequently, this route enabled ROC curve analyses, as described below.
– **Analysis Route 2:** Algebraic image reconstruction and analysis, including modelling of the device's spatial response function and homogeneous gamma-ray attenuation in the image reconstruction as well as more advanced image analysis tools to identify and quantify pin-shaped objects in the reconstructed image. This route was not automated and thus smaller populations of assemblies could be analysed (up to 10), excluding ROC curve analyses of the results.

Apart from demonstrating the methods' capabilities to distinguish diverted fuel pins from pins present, one important aspect of these studies was to compare the performance of the PGET and UGETv1 devices.

Examples of quantified pin-wise ^{154}Eu activities when applying the two alternative analyses routes on simulated UGETv1 data for short-cooled PWR fuel assemblies with missing pins, offering a challenging diversion scenario for the most challenging fuel type of the three under study, are presented in Figure 8. As seen in the figure, the FBP reconstruction (which does not take gamma-ray attenuation into account) calculates lower pin activities in the assembly interior than in its periphery, whereas a more leveled response is given by the model-based algebraic reconstruction (which takes gamma-ray attenuation into account). In agreement with ref. [19], model-based reconstruction seems to allow for better separation between fuel pins and missing pins and/or water channels. However, one should also note that the simulation for the latter does not include any pin-BU variation.

ROC curve formalism (see section 6) was used to compare the expected performance of the existing PGET device with that of the notional UGETv1 device. For both devices, perfect energy and efficiency calibration of detector elements was assumed in the simulations. The evaluations were based on automated FBP reconstruction and summation of pixel values (Analysis Route 1) for sets of 1,000 virtual fuel assemblies with a BU variation for each pin selected from a uniform distribution within ±20% of the nominal value and stochastic noise corresponding to a 60-minute assay for UGETv1 and a 10-min assay for PGET. The results for the three fuel types under study with fuel parameter sets {BU=20 GWd/MTU, CT=5 years} and {BU=10 GWd/MTU, CT=40 years} are presented in Figure 9. For the sets with CT=5 years, the 1274-keV radiation from ^{154}Eu was analysed, while the 662-keV radiation from ^{137}Cs was used for the sets with CT=40 years.

The ROC curves in Figure 9 indicate that PGET offers more confident or similar capability of detecting missing pins as UGETv1. However, one should also note that no ROC analyses have been made for Analysis Route 2, which might offer different detection capability according to the results in Figure 8. The detection capability is further discussed in section 7.5.

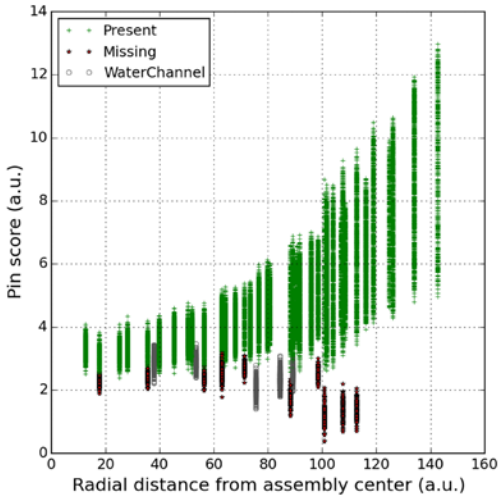

Radial distance from assembly centre (a.u.)

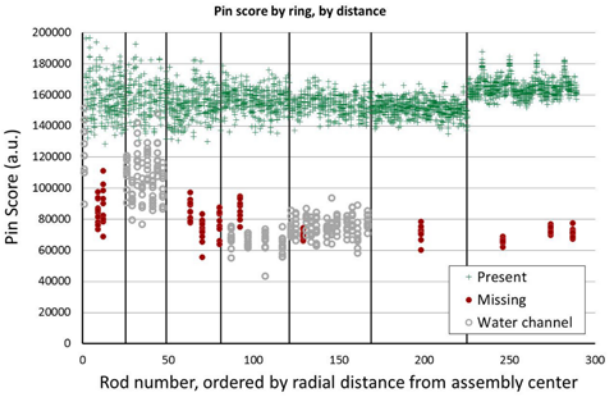

Pin number, ordered by ring, by radial distance from assembly centre (a.u.)

Figure 8: Pin-scores for pins present and pins missing, simulating the deployment of the UGETv1 device on sets of PWR assemblies (BU=40 GWd/MTU, CT=1 year) using the 1275 keV emission from ^{154}Eu. The upper figure results from simple FBP reconstruction and pixel summation on a set of 100 virtual assemblies with ±20% pin-wise BU variation. The lower figure results from model-based algebraic reconstruction and image analysis on a set of 10 virtual assemblies with no pin-wise BU variation. (Since the lower figure is the aggregate of 10 simulations, each of fuel with 253 pins present, 11 pins missing and 25 water channels, it contains markers for in total 2783 pins present, 110 pins missing and 275 water channels.) Both data sets include stochastic noise.

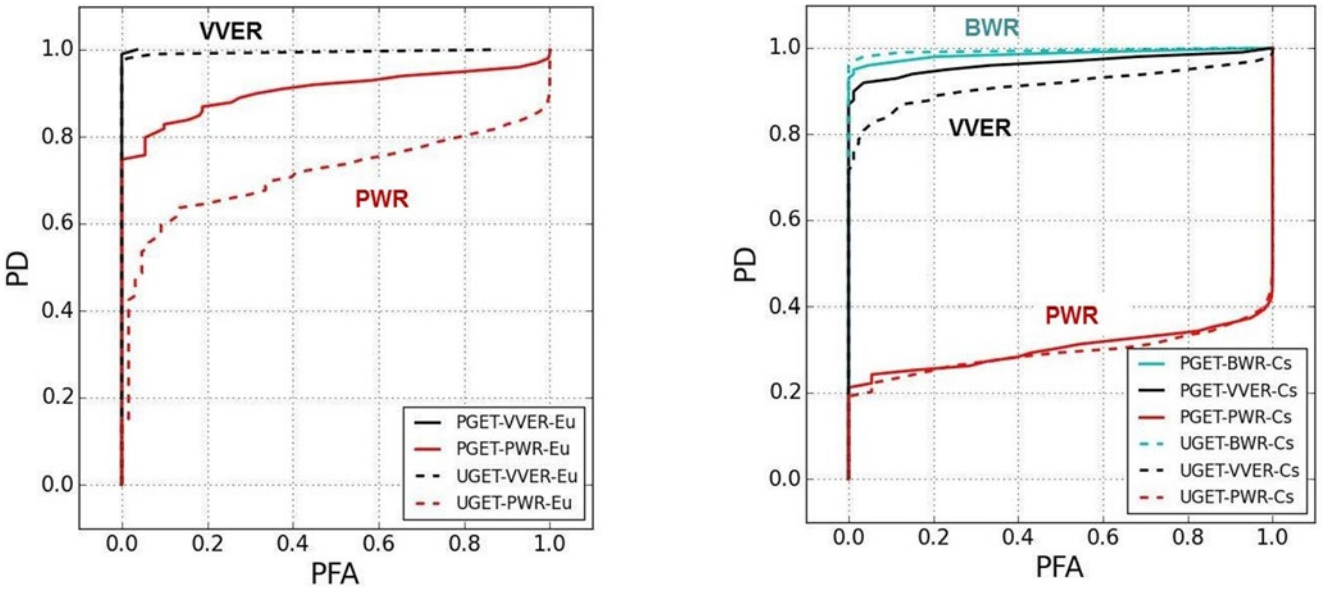

Figure 9: Predicted detection sensitivity of a single missing pin (i.e., bias defect) for perfectly-calibrated PGET and UGETv1 for BWR, VVER and PWR fuels, deploying simple FBP reconstruction and pixel summation. **Left:** Nominal BU of 20 GWd/MTU and 5 year CT with assay based on ^{154}Eu. (BWR performance is even higher than VVER and therefore not shown.) **Right:** Nominal BU of 10 GWd/MTU and 40-year CT with assay based on ^{137}Cs.

7.4 Results for Verification Objective 2: Pin-wise fuel properties

Verification Objective 2 assumes availability of the fuel-geometry information needed to enable the detailed algebraic reconstruction methods described in section 5.2. Using these methods, pin-wise isotopic contents are reconstructed (rather than images as in Verification Objective 1). The quality of the results, i.e. the precision of the calculated pin-wise isotopic contents, will depend on the fidelity of the algebraic system matrix. If spectroscopic full-energy peak analysis is applied, such as in the notional UGETv1 design (see section 2.2), full fidelity may be provided by full-energy transport calculations (ray tracing). If the collected data comprises significant object-scattered components, which may be the case for the PGET design, the calculations may require the inclusion of gamma-ray scattering as well. However, the more detail that is included in the calculations, the longer the execution time, which may make the most detailed calculations, such as MCNP, prohibitively long.

The results from three types of analyses are presented below;

1. Pin-wise isotopic-content reconstructions using the ray-tracing toolkit TOMOPACK, applied to simulated data for the notional UGETv1 device design for PWR fuel assemblies;
2. Pin-wise isotopic-content reconstructions using the RADSAT toolbox, which includes calculations of gamma-ray scattering components, applied on simulated data for the notional UGETv1 device design and the existing PGET device.
3. Estimation of pin-wise BU and CT, based on measured pin-wise isotopic contents.

For a complete description of all analyses performed, we refer to [10].

7.4.1 Ray-tracing-based reconstruction models

Simulations of UGETv1 assay of PWR fuel assemblies with 11 fuel pins missing (see Figure 7) have been analysed using the TOMOPACK ray-tracing-based reconstruction toolkit. In the simulations, the assemblies contained uniform pin-wise isotopic contents, and sets of 10 virtual assemblies were analysed for each case under study. Results for a short-cooled (1 year), high-BU PWR assembly (40 GWd/MTU) with 11 fuel pins missing are presented in Figure 10. Reconstructed relative pin-by-pin isotopic contents of ^{137}Cs, ^{134}Cs and ^{154}Eu are presented in terms of the fractional error from the simulated values, ordered ring-by-ring from the fuel assembly centre to the periphery. In the presented cases, the level of statistics in the analysed data sets corresponds to 40 minutes total assay time. Since a prerequisite for Verification Objective 2 was a priori known fuel geometry, activities are only reconstructed in fuel pins present and not in water channels or positions of missing pins.

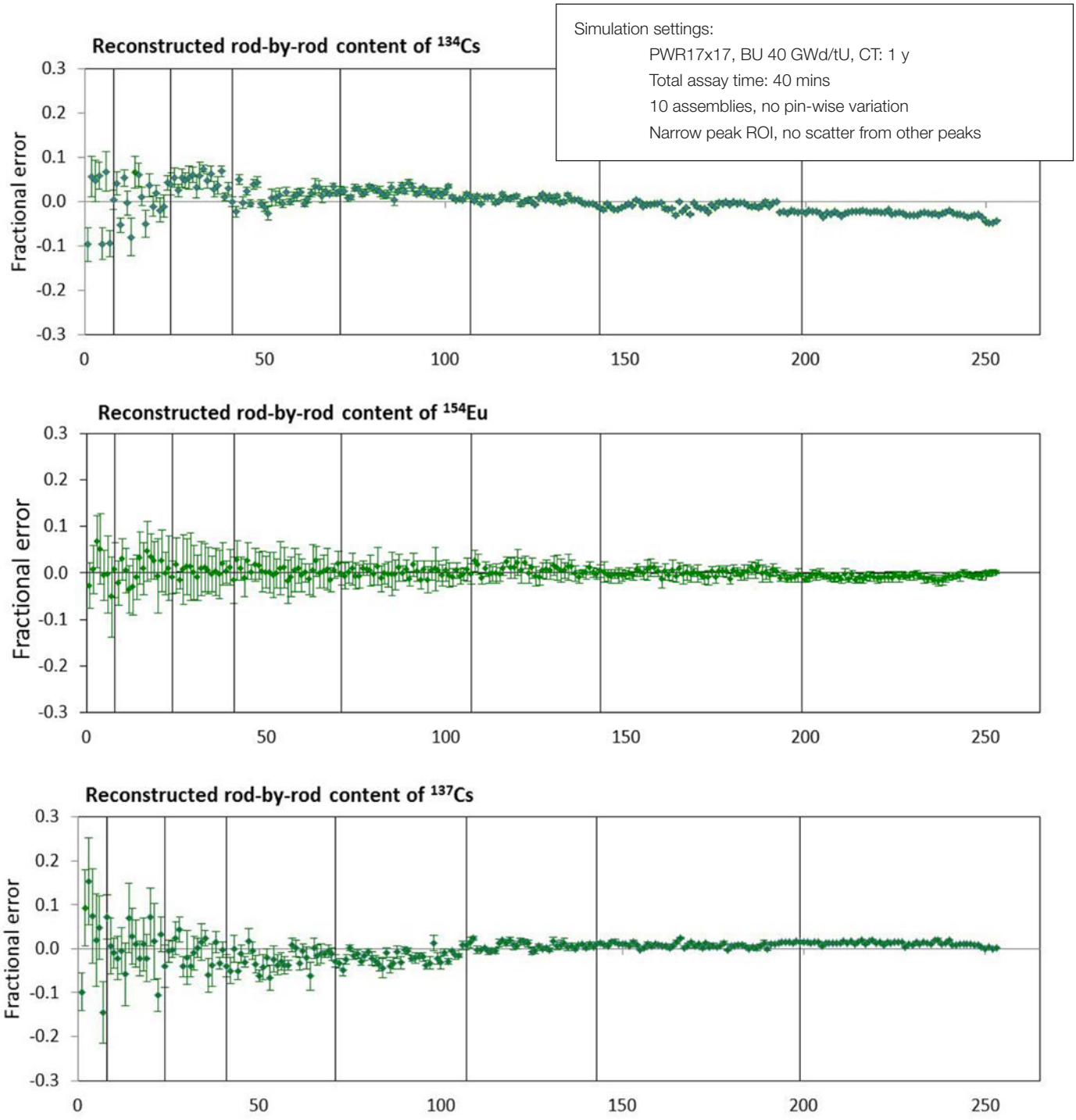

Figure 10: Results obtained in TOMOPACK reconstructions of simulated data for short-cooled, high-BU PWR 17x17 fuel assemblies in the suggested UGETv1 device design, presented as mean values of fractional error in reconstructed pin-by-pin isotopic contents obtained in analyses of 10 datasets, including error bars corresponding to ±1 σ confidence intervals. All pins were assigned equal isotopic contents in the simulations. The analyses were based on full-energy gamma peaks at 662 keV (^{137}Cs), 796 keV (^{134}Cs) and 1274 keV (^{154}Eu).

For all three isotopes in Figure 10, precision is high in peripheral fuel pins and up to about 10% (1 σ) in central fuel pins. Systematic deviations are generally smaller than a few %, except for the most central sections, where insufficient sampling of single-pin base sinograms may disturb the analysis (see section 3). The best and most stable results are obtained for ^{154}Eu, which emits the highest gamma-ray energy (1274 keV) and thus offers the highest escape fraction from the assembly centre.

The TOMOPACK ray-tracing toolkit was also used for reconstructing the pin-wise content of ^{137}Cs based on simulations of long-cooled (40 years) low-BU (10 GWd/MTU) PWR fuel. In this "difficult" case (low source concentration, low gamma-ray energy, large-sized fuel), longer measurement times would be required to obtain good statistics, and approximately 2 hours total assay time would give similar results as presented in Figure 10 (top).

7.4.2 Reconstruction models including scattered components

The RADSAT-based reconstruction approach offers a possible means to introduce scattering components when defining the system matrix, which may be valuable for the analyses of PGET data, in particular when broad energy windows are deployed so that object scatter constitutes a significant portion of the sinogram signal. Here, RADSAT has been used to analyse simulated data for both the UGETv1 and the PGET device. Data sets from 100 virtual VVER assemblies were studied, including ±20% variation in pin BU and six tampered fuel pins with 50% of the average BU value (replicating material diversion at about mid-life of the fuel). Figures 11 and 12 show the results for pin-by-pin quantification of the ^{137}Cs and ^{154}Eu concentrations in VVER fuel with two sets of fuel parameters; {BU=20 GWd/MTU, CT=5 years} and {BU=10 GWd/MTU, CT=40 years}. As described in section 7.2, relatively broad ROI were used when simulating PGET data, while UGETv1 data were simulated assuming spectroscopic full-energy peak analysis with background subtraction.

As seen in Figure 11 (top) and Figure 12 (top), RADSAT calculates activities in normal fuel pins within a few percent for all VVER fuels under study, when applied on simulated data for the UGETv1 device. Statistical uncertainty is smaller in the assembly periphery (as expected), but also in the inner sections precision is in the order of a few percent. Some systematic deviations may be identified, but these are also on the few-percent level. Performance is good also for tampered fuel pins, although their content of ^{154}Eu is generally slightly overpredicted and the statistical uncertainty is higher than for normal fuel pins. Accordingly, one would expect these tampered fuel pins to be confidently detected. In addition, a short-CT (1 year), high-BU (40 GWd/MTU) fuel was studied, giving similar results for ^{154}Eu assay using UGETv1 as presented in Figure 11 (top). (For this short-cooled fuel, only UGETv1 assessment was covered because PGET cannot manage the high count rates encountered for such fuel.)

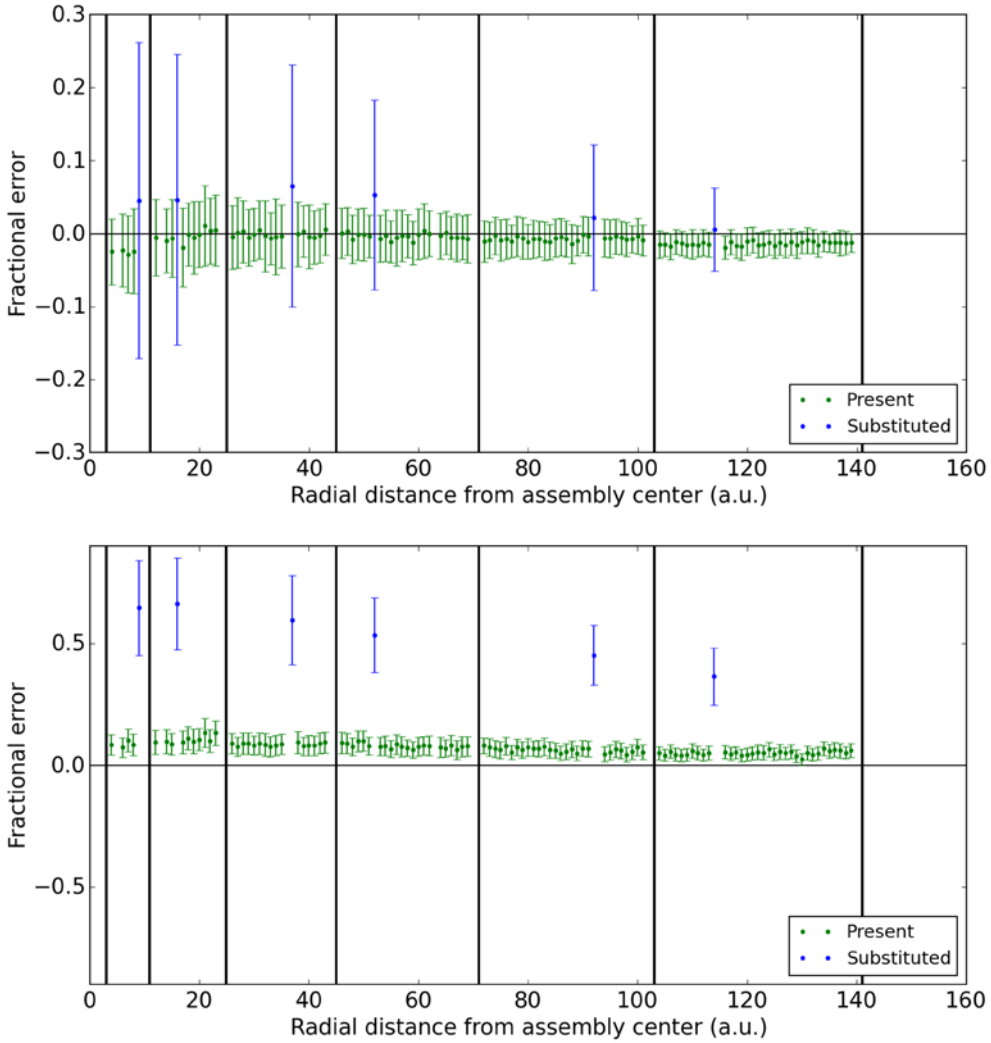

Figure 11: Fractional error, relative to true values, for pin-by-pin ^{154}Eu activity reconstruction with RADSAT-based system matrix using UGETv1 (top panel) and PGET (bottom panel). The 100-assembly population assumed VVER fuel with nominal BU of 20 GWd/MTU, 5-year CT, and ±20% pin-wise BU variation. Tampered pins (blue), have a nominal activity half that of the pins present (green). Error bars represent 1 σ uncertainties, obtained based on the simulated fuel population.

In the analyses of simulated data for the PGET device, there is a systematic overprediction of the activities in normal fuel pins, which increases towards the assembly centre. The tampered fuel pins are strongly overpredicted, especially for the ^{154}Eu assessment in Figure 11 (bottom), which would complicate their detection. Alternative ways to improve this situation could be to (i) analysis-wise further enhance the modelling capabilities for scattering, or (ii) measurement-wise define energy windows such that scattering components in the data are minimized. While the latter alternative may be applicable to ^{137}Cs data, the low full-energy detection efficiency at 1274 keV of the PGET detector elements may preclude such an approach for ^{154}Eu data.

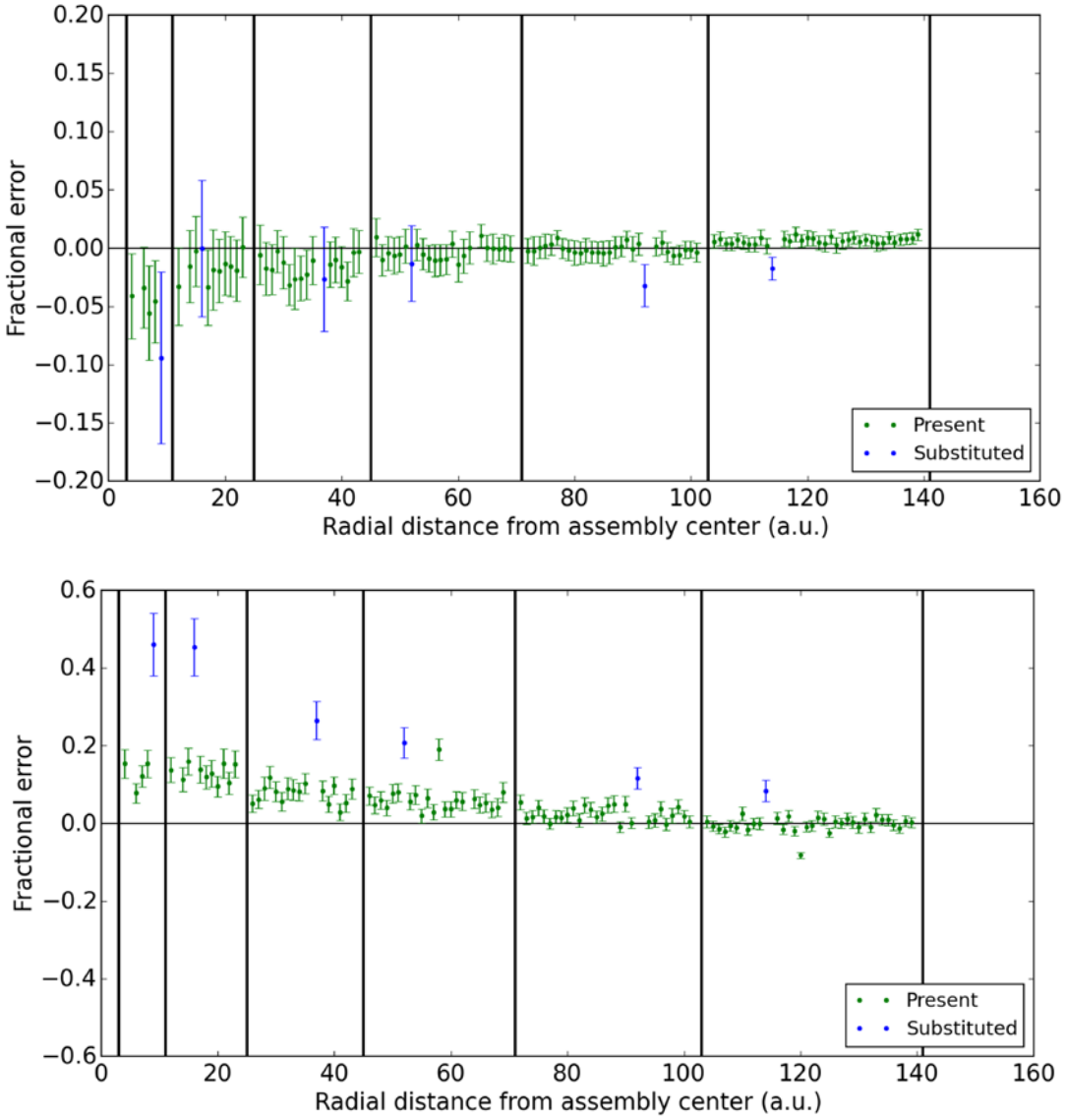

Figure 12: Fractional error, relative to true values, for pin-by-pin ^{137}Cs activity reconstruction with RADSAT-based system matrix using UGETv1 (top panel) and PGET (bottom panel). The 100-assembly population assumed VVER fuel with nominal BU of 10 GWd/MTU, 40-year CT and ±20% pin-wise BU variation. Tampered pins (blue), have a nominal activity half that of the pins present (green). Error bars represent 1 σ uncertainties, obtained based on the simulated fuel population.

7.4.3. Pin-wise BU and CT determination

Gamma-ray spectroscopy is an established technique to characterize nuclear fuel, and several studies have been made to establish correlations between full-energy peak intensities of gamma rays from ^{137}Cs, ^{134}Cs and ^{154}Eu, recorded in gamma-scanning measurements of nuclear fuel assemblies, to fuel parameters such as BU and CT [24]. In a similar manner, tomographically measured pin-wise activities of these isotopes may be used to determine BU and CT on the single-pin level. These pin-wise fuel parameters may, in turn, be used to control the consistency of the population of fuel pins in an assembly or even to verify operator-declared data, if available on the single-pin level. However, such data are not typically provided to the IAEA today in spent fuel declarations.

As described in [10], the investigations performed in this work lead to the following conclusions;

– For short-cooled fuels, analysis of the quotients of the tomographically measured pin-wise contents of ^{134}Cs and ^{154}Eu would offer the smallest statistical uncertainty in the determination of pin-wise BU and CT, using the methods in [24], when these isotopes are available (i.e. at CT<10 years).
– At intermediate CT (10 to 30 years), the quotient of ^{154}Eu and ^{137}Cs can be used, with slightly larger statistical uncertainties.
– At long CT (>30 years), only ^{137}Cs will be available. However, ^{137}Cs can still give a direct measure of the fuel BU, provided that all fuel pins have the same CT. Consequently, the precisions demonstrated in e.g. Figure 10 (top) or Figure 12 (top) give a direct measure of the achievable precisions in pin-wise BU determination.

Considering a 40-minute assay using the notional UGETv1 device, the simulations and ray-tracing-based analyses in this work (see section 7.4.1) show that even for the innermost sections of PWR fuel assemblies with CT=1 year and BU=40 GWd/MTU, the pin-wise BU and CT may be determined with statistical uncertainties below 6% and 0.4 years, respectively, based on the quotients of the pins' ^{134}Cs and ^{154}Eu contents. However, one should note that this represents the highest achievable precision, which requires that systematic uncertainties are eliminated. For more information, we refer to [10].

7.5 Discussion on predicted UGETv1 and PGET performance

As seen in Figure 9, the evaluations on Verification Objective 1 indicate that PGET performance would exceed that of UGETv1 for most analysed cases. The reason is mainly the larger number of detector elements in PGET, which leads to more efficient data collection and thus to better counting statistics during a fixed measurement time. Assuming an operationally tolerable false alarm rate of approximately 0.05 (1 false alarm per 20 assemblies), these findings indicate that Analysis Route 1 (FBP reconstruction and summation of pixel values) would achieve a probability of detecting a single missing pin, at any location in the assembly, that is greater than 0.80 for VVER and BWR fuels, with both devices, regardless of BU and CT. However, the evaluation also indicates that the single-missing-pin performance for both devices would be low for PWR fuel (due to its large physical dimension and relatively tight fuel-pin spacing). Referring to Figure 8, one should note that alternative analyses, such as Analysis Route 2 (algebraic reconstruction and advanced image analysis) may perform better, albeit efforts must be made to automate it for use in unattended mode.

As seen in Figure 11 and 12, the evaluations on Verification Objective 2 indicate superior performance of the UGETv1 device as compared to PGET, contrary to Objective 1. The reason is the capability of UGETv1 to select full-energy gamma, which enables the analysis of isotope-specific data. However, one may expect that smaller energy windows (for example 630-680 keV instead of 400-700 keV for ^{137}Cs, which was simulated here), may help to reduce the systematic bias in the application of PGET to Objective 2. More investigations of object-scatter effects, as a function of energy-window width in PGET, are needed. For UGETv1, a potential to deduce pin-wise BU and CT in short-cooled PWR fuel with statistical uncertainties below 6% for BU and below 0.4 years for CT, has been indicated even for central pins.

Finally, one should note that PGET is not operational at CTs down to 1 year due to count-rate saturation of the detector elements in the high gamma flux from short-cooled fuel, while UGETv1 was designed to be operational also at short CTs. For Verification Objective 1, results obtained when applying Analysis Route 1 on UGETv1 data at CT=1 year shows that a probability >95% for detecting a single missing fuel pin would be achievable for all three fuel types under study, assuming a tolerable false alarm rate of 0.10. For more detailed information of these analyses, we refer to [10].

8. Envisaged inspection procedure

The envisioned inspection procedure, identified and refined as part of the JNT 1955 Phase I project can be outlined according to the following:

A. Baseline inspection procedure, performed on-site, either automatically in case of unattended use or by an inspector in the case of attended use:

1. Tomographic measurement
2. Online image reconstruction
3. Online image analysis
4. On-site initial integrity statement

B. If undeclared removal/replacement is suspected:

5. Detailed pin-activity reconstruction based on current fuel type and position in device. (No additional measurement required.)

The last step (B.5) reflects the functionality of Verification Objective 2, at least if operator-declared information is used for the detailed modelling. However, it may also be envisaged that geometric information is extracted directly from reconstructed images in step A.2, without any need for operator-declared data. Such a possible procedure ("Verification Objective 1.5") is also discussed below.

9. Conclusions, discussion and outlook

According to this and previous studies, GET has the potential to provide bias-defect sensitivity in most fuel verification scenarios, a significant improvement over IAEA's current partial-defect capabilities using a Fork-based system or Digital Cerenkov Viewing Device. The IAEA also possesses a GET measuring device for attended use (PGET). This device was refurbished during 2016, introducing e.g. new detector elements and data-acquisition electronics in order to provide adequate efficiency and energy calibration; capabilities which did not meet expectations before refurbishment. The current study covers analyses of expected PGET performance, based on simulations for a variety of fuel types and fuel parameter sets, assuming high-fidelity calibration but based on the detailed design before refurbishment. Because only minor changes were made to the detector elements, the results are expected to be representative for the refurbished PGET. However, there may still be room for improvements in terms of e.g. optimisation of energy windows used for selecting the detected gamma rays to be analysed, which can be a subject for future studies.

In this study, a "Universal" GET design has been developed ("UGETv1"), which is capable of supporting the full range of fuel characteristics considered in this study, but that versatility comes at a price in terms of both assay time and instrument lifecycle cost. (For cost estimates, see [10].)

A set of tomographic reconstruction algorithms has been identified, described and used, which may find use in the application of GET for safeguards. For Verification Objective 1 (counting of fuel pins without any prior information on the fuel), image reconstruction algorithms have been presented, which are complemented by image-analysis methods to count the number of fuel pins present in the measured assembly. For Verification Objective 2 (determination of pin-wise fuel properties, making use of prior information on e.g. fuel geometry), algebraic methods have been suggested that include detailed modelling of the gamma-ray transport through the fuel configuration.

Among the outcomes of this work is the creation of a simulation and modelling framework, which provides end-to-end capability to assess tomographer performance for nuclear fuel assay, and could be considered a new, standing capability for the international safeguards community, available on request. It is modularised to allow for studies of expected performance of various GET measurement device designs for a variety of fuel types, fuel properties and data analysis methods.

For Verification Objective 1, it was found that the PGET and UGETv1 devices exhibit, in general, comparable performance despite their very different designs, but PGET achieves that sensitivity in shorter assay times. The higher collection efficiency of PGET elevates its performance over UGET for cases where the signal coming from interior pins is particularly weak (e.g., PWR assemblies), while UGET achieves high performance for the shortest-cooled fuels that cannot be measured by PGET. These comparative findings are based on an analytic FBP reconstruction; however, results may vary with other reconstruction methods. One may e.g. note that algebraic reconstruction including modelling of the system's intrinsic response function and uniform attenuation gave the most promising results in terms of separation between fuel pins and background, see e.g. Figure 8. Prior work has also indicated that image analysis and algebraic reconstruction methods offer the potential robustness to issues such as misalignment of assemblies, bowing of individual fuel pins, non-functioning detector elements, irregular measurement positions etc.

For Verification Objective 2, predicted performance for PGET was lower than for UGETv1, primarily because significant object-scatter contributions in PGET's wide energy windows perturb a relatively small full-energy peak signal. Smaller energy windows might offer improvements in Objective 2 performance for PGET, but more studies are needed to quantify this potential. It may also be envisaged that geometric information may be extracted from reconstructed Objective 1-type images, to be used in Objective 2-type analyses without any need for operator-declared data. The project team and stakeholders have discussed the potential for such a procedure ("Verification Objective 1.5"), but analysis of such an approach was beyond the scope of this study.

Finally, one may note that the performance metric used for Verification Objective 1 relates to bias defects, i.e. diversion of single fuel pins. If the performance metric were defined for higher defect levels (e.g. 5% or 10% of the pins instead of the <0.5% bias defect at the event of 1 missing pin out of 264 pins in a PWR assembly) the ROC curves are expected to look considerably better also for PWR fuels. This is an area for future work.

10. Acknowledgements

U.S. participation in the JNT 1955 Phase I project has been funded by the U.S. Support Program to the International Atomic Energy Agency (IAEA) and the National Nuclear Security Administration's Office of Nonproliferation and Arms Control. Uppsala University's contributions were funded by the Swedish Radiation Safety Authority (SSM) via the Swedish Support Program to the IAEA under contracts SSM2013-85-9, SSM2014-94, SSM2015-99, SSM2016-130, and activity number 3060152-08. The computations performed by Uppsala University were partially performed on resources provided by Swedish National Infrastructure for Computing (SNIC) through Uppsala Multidisciplinary Center for Advanced Computational Science (UPPMAX) under projects p2013091, snic2013-1-296, snic2014-1-203, and snic2014-1-392. Finnish participation was supported by the Finnish Support Program to the IAEA, financed by the Finnish Foreign Ministry. The contribution by the European Commission was financed through the regular European Commission budget.

The project team appreciates the guidance of IAEA's James Ely, Misha Mayorov, and Alain Lebrun.

11. References

[1] International Atomic Energy Agency; *Special Criteria for Difficult-to-Access Fuel Items*; SG-GC-Annex-04; IAEA; 2009.

[2] International Atomic Energy Agency; *IAEA Department of Safeguards Long-Term R&D Plan, 2012-2023*; STR-375; IAEA; 2013.

[3] Lévai F, Desi S, Czifrus S, Feher S, Tarvainen M, Honkamaa T, Saarinen J, Larsson M, Rialhe A and Arlt R; *Feasibility of gamma emission tomography for partial defect verification of spent LWR fuel assemblies*; STUK-YTO-TR-189; Finnish Radiation and Nuclear Safety Authority, STUK; 2002.

[4] Honkamaa T, Levai F, Turunen A, Berndt R, Vaccaro S, and Schwalbach P; *A Prototype for passive gamma emission tomography*; IAEA Safeguards Symposium; 2014.

[5] Jacobsson Svärd S, Håkansson A, Bäcklin A, Osifo O, Willman C and Jansson P; *Non-destructive Experimental Determination of the Pin-power Distribution in Nuclear Fuel Assemblies*; Nuclear Technology, 151(1):70-76; 2005.

[6] Jansson P, Jacobsson Svärd S, Håkansson A and Bäcklin A; *A Device for Non-destructive Experimental Determination of the Power Distribution in Nuclear Fuel Assemblies*; Nuclear Science and Engineering 152(1):76 86; 2006.

[7] Jacobsson Svärd S, Håkansson A, Bäcklin A, Jansson P, Osifo O and Willman C; *Tomography for partial-defect verification - experiences from measurements using different devices*; ESARDA Bulletin, 33:15-25; 2006.

[8] Baird B; *Quantitative analysis of the fission product distribution in a damaged fuel assembly using gamma-spectrometry and computed tomography for the Phebus FPT3 test*; Nuclear Engineering and Design, 262:469-483; 2013.

[9] Holcombe S, Jacobsson Svärd S and Hallstadius L; *A novel gamma emission tomography instrument for enhanced fuel characterization capabilities within the OECD Halden Reactor Project*; Annals of Nuclear Energy, (85):837–845; 2015.

[10] Smith LE, Jacobsson Svärd S, Mozin V, Jansson P, Miller E, Honkamaa T, Deshmukh N, White T, Wittman R, Trellue H, Grape S, Davour A, Andersson P, Holcombe S and Vaccaro S; *A Viability Study of Gamma Emission Tomography for Spent Fuel Verification: JNT 1955 Phase I Technical Report*; PNNL-25995, Pacific Northwest National Laboratory, USA; 2016.

[11] Trellue HR, Fensin ML, Richard JR, Galloway J and Conlin JL; *Description of the Spent Nuclear Fuel Used in the Next Generation Safeguards Initiative to Determine Plutonium Mass in Spent Fuel*; LA-UR 11-00300, Los Alamos National Laboratory, USA; 2011.

[12] Mozin V and Tobin S; *DGSDEF: Discrete Gamma-ray Source DEFinition code*; LA-CC-10-083. Los Alamos National Laboratory, USA; 2010.

[13] Pelowitz DB; *MCNPXTM User's Manual. Version 2.6.0*; NM LA-CP-07-1473 Los Alamos National Laboratory, USA; 2008.

[14] Agostinelli A et.al.; *Geant4 a simulation toolkit*; Nuclear Instruments and Methods in Physics Research Section A, 506:250–303; 2003.

[15] C. Netterbrandt, Oskarshamns Kraftgrupp AB (OKG), Personal communication, March 2014.

[16] J. Eriksson, Forsmarks Kraftgrupp AB (FKA), Personal communication, March 2014.

[17] White TA, Jacobsson Svärd S, Smith LE, Mozin VV, Jansson P, Davour A, Grape S, Trellue N, Deshmukh NS, Wittman RS, Honkamaa T, Vaccaro S and Ely JH; *Passive Tomography for Spent Fuel Verification: Analysis Framework and Instrument Design Study*; ESARDA Symposium, Manchester, UK; 2015.

[18] Kak AC and Slaney M; *Principles of Computerized Tomographic Imaging*; IEEE Press, ISBN 0-85274-349-1, Piscataway, NJ, USA; 1988.

[19] Jacobsson Svärd S, Holcombe S and Grape S; *Applicability of a set of tomographic reconstruction algorithms for quantitative SPECT on irradiated nuclear fuel assemblies*; Nuclear Instruments and Methods in Physics Research Section A, 783:128–141; 2015.

[20] Davour A, Jacobsson Svärd S, Andersson P, Grape S, Holcombe S, Jansson P and Troeng M; *Applying image analysis techniques to tomographic images of irradiated nuclear fuel assemblies*; Annals of Nuclear Energy, 96:223-229; 2016.

[21] Shaver MW, Smith LE, Pagh RT, Miller EA, and Wittman RS; *The Coupling of a Deterministic Transport Field Solution to a Monte Carlo Boundary Condition for the Simulation of Large Gamma-Ray Spectrometers*; Nuclear Technology 168(1):95-100; 2009.

[22] Metz CE; *Basic Principles of ROC Analysis*; Seminars in Nuclear Medicine; 8(4):283-298; 1978.

[23] IAEA Nuclear Data Section, Isotope Browser. Updated 2017.

[24] Jansson P. *Studies of Nuclear Fuel by Means of Nuclear Spectroscopic Methods*; PhD thesis, Uppsala University, Sweden. Retrievable at http://urn.kb.se/resolve?urn=urn:nbn:se:uu:diva-2057; 2002.